OPEN ACCESS

Applied Physics Express **19**, 116501 (2026)

LETTER

https://doi.org/**10.35848/1882-0786/aebde4**

Demonstration of β-Ga_2O_3 MEMS resonators fabricated by crystallographic gas etching of (001) β-Ga_2O_3 substrates

Takayoshi Oshima[1*], Yuichi Oshima[1], Yuto Amano[2], Masataka Imura[1], Meiyong Liao[1], and Ya Zhang[2]

[1]*Research Center for Electronic and Optical Materials, National Institute for Materials Science, Tsukuba, Ibaraki 305-0044, Japan*
[2]*Institute of Engineering, Tokyo University of Agriculture and Technology, Koganei, Tokyo 184-8588, Japan*

[*]E-mail: OSHIMA.Takayoshi@nims.go.jp

Received October 12, 2026; accepted November 3, 2026; published online November 11, 2026

We report the first resonance characterization of β-Ga_2O_3-based doubly-clamped-beam resonators elongated along [100] and fabricated directly on a (001) β-Ga_2O_3 substrate by crystallographic gas etching. The beams exhibited clear fundamental-mode resonances with quality factors (Q) on the order of 10^4. Analysis of the beam-length dependence of the resonant frequency (f_0) yielded an effective Young's modulus of 143.2 (+16.4/−14.0) GPa within the Euler–Bernoulli beam approximation, while axial-stress analysis indicated only a small residual tensile stress. The f_0Q values exceeded the highest reported values for transferred-flake-based doubly clamped beams, highlighting the potential advantage of crystallographic etching for fabricating β-Ga_2O_3 microelectromechanical systems. © 2026 The Author(s). Published on behalf of The Japan Society of Applied Physics by IOP Publishing Ltd

Supplementary material for this article is available online

Wide-bandgap semiconductor microelectromechanical systems (MEMS) have attracted attention for harsh-environment sensors, high-frequency resonators, and mechanically functional components integrated with wide-bandgap electronics. SiC MEMS have been widely studied for harsh-environment sensing owing to their high thermal and chemical stability.[1,2] GaN MEMS have also been investigated as high-frequency resonators and piezoelectrically transduced MEMS devices,[3] while diamond MEMS have demonstrated excellent mechanical performance based on their high stiffness, thermal conductivity, and chemical stability.[4,5] These studies indicate that wide-bandgap semiconductors can expand MEMS technologies beyond the operating limits of conventional Si-based MEMS.

In this context, β-Ga_2O_3 is also an attractive ultrawide-bandgap semiconductor for MEMS applications beyond conventional Si platforms. Its wide band gap of $\geqslant 4.43$ eV[6] gives rise to a high critical electric field of >6 MV cm^{-1} [7,8] and intrinsic solar-blind sensitivity below 280 nm,[9] making β-Ga_2O_3 promising for power electronics and deep-ultraviolet optical applications.[10] In addition, β-Ga_2O_3 has been investigated for gas sensors based on its sensitivity to oxidizing and reducing gases.[11,12] Its tolerance to elevated temperatures and radiation further makes β-Ga_2O_3-based devices promising for harsh-environment operation.[13–16] Together with its mechanical properties comparable to those of Si, these features suggest that β-Ga_2O_3 could enable harsh-environment MEMS actuators and resonant sensors, as well as monolithically integrated mechanical components for β-Ga_2O_3-based electronic, optical, and sensing systems.[17] Furthermore, bulk β-Ga_2O_3 substrates can be grown by melt-based methods, offering advantages in substrate quality, scalability, and productivity.[18] Therefore, β-Ga_2O_3 is attractive as a native-substrate platform for integrated MEMS devices.

Despite these promising material and device features, β-Ga_2O_3 MEMS technology is still in an early stage of development. Several β-Ga_2O_3-based MEMS devices have been demonstrated, including nanomechanical resonators,[17,19,20] resonant ultraviolet sensors,[21,22] resonant gas sensors,[23] resonant pressure sensors,[24] vibrating channel transistors,[25] and thermal actuators.[26] Most of these devices, however, have relied on the transfer of β-Ga_2O_3 flakes onto foreign substrates.[17,19–22,24–26] Such transfer-based processes are useful for proof-of-concept demonstrations but are not ideal for reproducible and scalable MEMS fabrication.

Recently, crystallographic gas and wet etching have enabled the direct fabrication of β-Ga_2O_3/air-gap structures, such as cantilevers and doubly clamped beams, on bulk β-Ga_2O_3 substrates without using transfer processes.[27–29] In particular, the crystallographic gas-etching process and the resulting suspended structures used in the present study were established in our previous work.[27,28] However, their resonance characteristics have not yet been experimentally evaluated.

In this study, we report the first resonance characterization of monolithic doubly clamped beams directly fabricated on a (001) β-Ga_2O_3 substrate by crystallographic gas etching. We evaluate their fundamental-mode resonance behavior, quality factors, beam-length dependence of resonant frequency, and effective Young's modulus.

β-Ga_2O_3 doubly clamped beams with different lengths along the [100] direction were fabricated on a (001) β-Ga_2O_3 substrate (Novel Crystal Technology). The detailed fabrication sequence including laterally enhanced HCl gas etching was described in our previous study.[28] First, mesas were formed by laser lithography followed by inductively coupled plasma reactive-ion etching (ICP-RIE) using BCl_3 and Ar gases. The etching depth was 1.75 μm. After complete removal of the residual photoresist by organic-solvent cleaning, oxygen plasma ashing, and HNO_3 cleaning, a 142 nm-thick SiO_2 masking layer was deposited by plasma-enhanced chemical vapor deposition. The SiO_2 layer was then patterned by laser lithography followed by capacitively coupled plasma RIE using CHF_3 and N_2 gases so that the SiO_2 mask covered

Content from this work may be used under the terms of the Creative Commons Attribution 4.0 licence. Any further distribution of this work must maintain attribution to the author(s) and the title of the work, journal citation and DOI.

© 2026 The Author(s). Published on behalf of The Japan Society of Applied Physics by IOP Publishing Ltd

only the top and sidewall surfaces of the mesa structures. After complete removal of the residual photoresist by organic-solvent cleaning and oxygen plasma ashing, HCl gas etching was performed at 647 °C under an HCl partial pressure of 250 Pa for 11 min. Finally, the SiO_2 mask was removed by buffered hydrofluoric acid etching.

The structural features of the fabricated doubly clamped beams were characterized using scanning electron microscopy (SEM) and a focused-ion-beam–SEM (FIB–SEM) hybrid system, as shown in Fig. 1. Beams with the same width of 5.7 μm and eight different lengths (L = 27.5, 37.5, 47.5, 57.5, 67.5, 77.5, 87.5, and 97.5 μm) were prepared [Fig. 1(a)]. The beam sidewalls exhibited striations caused by ICP-RIE [Fig. 1(b)], which could potentially be reduced by optimizing the RIE conditions. The beam thickness (t) was determined to be 0.95 ± 0.05 μm from an FIB–SEM cross-sectional observation at one representative location [Figs. 1(c) and 1(d)]. The uncertainty mainly reflects the rough underside of the beam, which may be characteristic of HCl gas etching of the (001) plane. Although the use of a (100)-oriented substrate could provide a smoother HCl-gas-etched surface,[27] we chose (001)-oriented substrates because they are more suitable for practical device fabrication in terms of scalable substrate availability and compatibility with epitaxial growth and device processing.

The resonance characteristics were measured using a custom-built optical vibration measurement setup. The β-Ga_2O_3 substrate on which the doubly clamped beams were fabricated was cut into a rectangular chip (5.0 × 15.0 × 0.65 mm) and attached to a piezoelectric actuator (10.0 × 10.0 × 3.0 mm; PA4HKW, Thorlabs) with vacuum grease for mechanical excitation. The piezoelectric element of the actuator was made of lead zirconate titanate (PZT) and had a nominal resonant frequency of 160 kHz. The mounted sample was then placed in a vacuum chamber equipped with optical windows, and the chamber was evacuated using a turbomolecular pump backed by a diaphragm pump. The vacuum pressure was measured to be 2.6 × 10^{-2} Pa. This pressure range is expected to be sufficiently low for characterizing MEMS resonators while suppressing air damping.[30,31] The out-of-plane motion of the beams was measured using a laser Doppler vibrometer with a 632.8 nm He–Ne laser focused to a spot diameter of approximately 2 μm, which was sufficiently smaller than the beam width. Resonance spectra were obtained by sweeping the driving frequency (f) applied to the piezoelectric actuator and recording the vibration amplitude (A) of the beams.

The fabricated beams exhibited clear resonance behavior. Fundamental-mode resonances were observed for beams with L = 47.5, 57.5, 67.5, 77.5, 87.5, and 97.5 μm. In contrast, the resonances of the shortest and second-shortest beams with L = 27.5 and 37.5 μm could not be measured, presumably due to insufficient excitation by the piezoelectric actuator at their expected resonance frequencies (f_0) of 6.55 and 3.52 MHz, respectively, estimated using the Euler–Bernoulli beam theory. Nevertheless, the obtained resonance curves of the longer beams were sufficiently clear for extracting the f_0 and quality factor (Q), as shown in Fig. 2. These parameters were extracted by fitting the resonance spectra using the frequency-response function of a damped harmonic oscillator:[32]

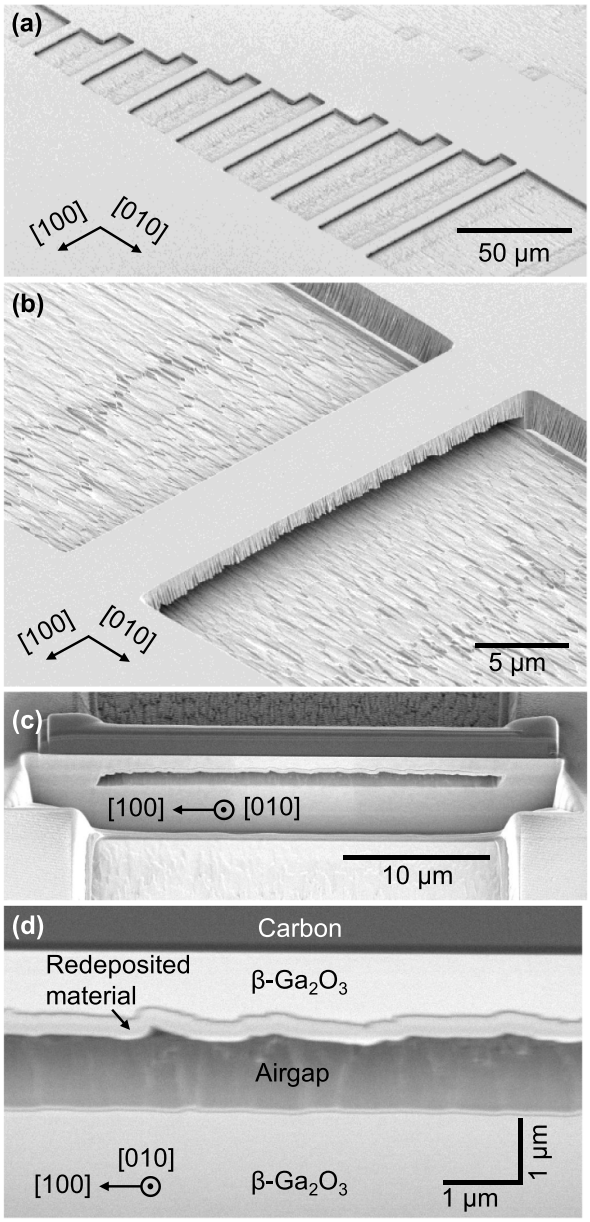


Fig. 1. Summary of scanning electron microscopy observations. (a) Surface-view image of β-Ga_2O_3 doubly clamped beams fabricated on a (001)-oriented β-Ga_2O_3 substrate. (b) Magnified image of the shortest beam. (c) Cross-sectional image of the beam with a focused-ion-beam-exposed cross section parallel to the (010) plane. (d) Magnified image of (c). All images were obtained at a tilt angle of 54°.

$$A\left(f\right) = \frac{B}{\sqrt{\left[1-\left(\frac{f}{f_0}\right)^2\right]^2 + \left(\frac{f}{f_0 Q}\right)^2}} + A_{\mathrm{bg}},$$

where B and A_{bg} are a frequency-independent amplitude scaling coefficient and a background offset, respectively. The obtained Q values were relatively high, on the order of 10^4, for all the measured beams. The Q values tended to decrease with increasing f_0. A Zener thermoelastic-damping analysis reproduced this qualitative trend as shown in Fig. S1 in the online supplementary data at https://stacks.iop.org/APEX/19/116501/mmedia/, although the calculated quality factor limited by thermoelastic damping values were several times

© 2026 The Author(s). Published on behalf of The Japan Society of Applied Physics by IOP Publishing Ltd

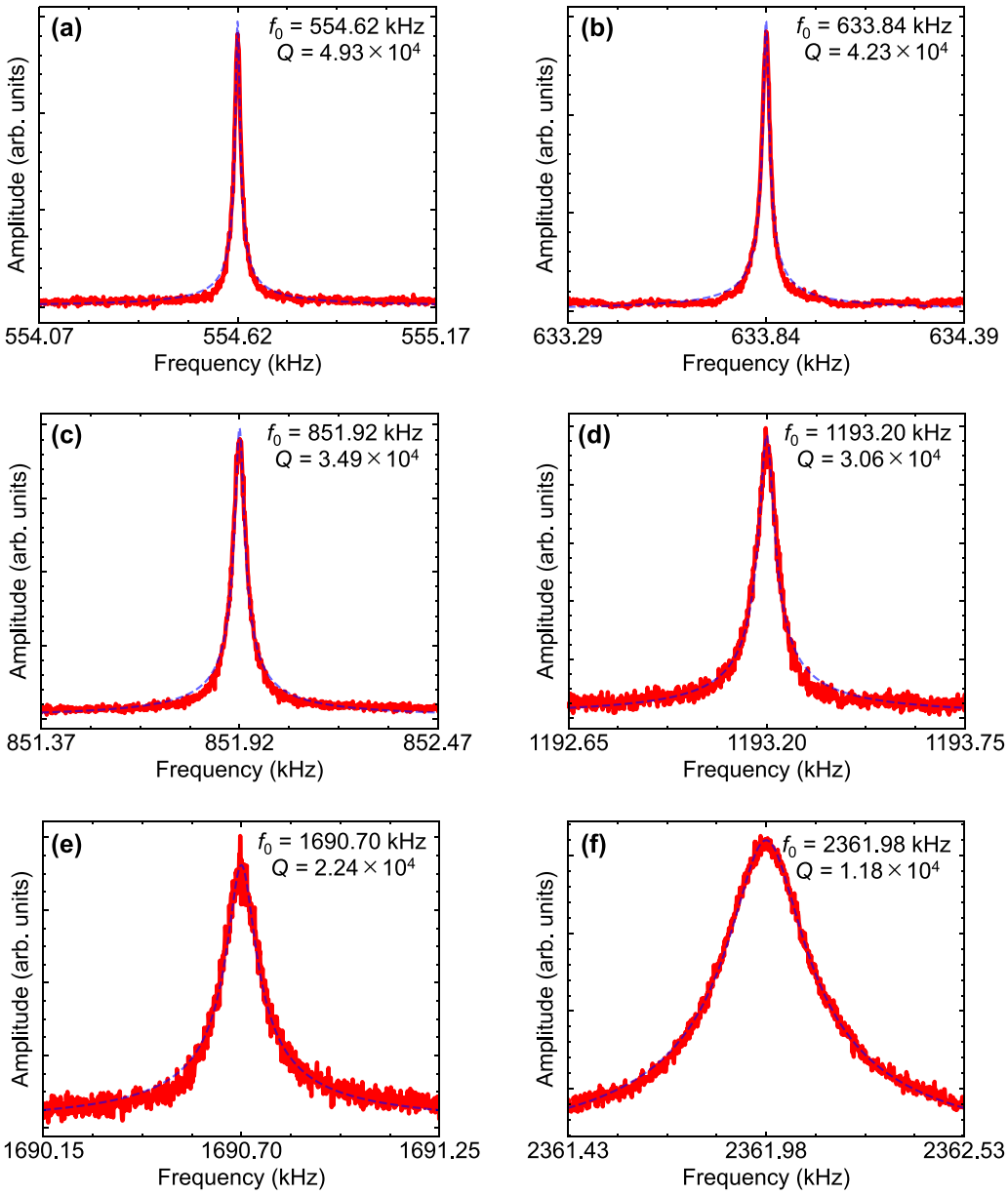


Fig. 2. Typical resonance spectra of doubly clamped beams with different beam lengths: (a) 97.5 μm, (b) 87.5 μm, (c) 77.5 μm, (d) 67.5 μm, (e) 57.5 μm, and (f) 47.5 μm. Red solid and blue dashed lines indicate measured and fitted data, respectively. f_0 and Q indicate resonant frequency and quality factor, respectively.

higher than the measured Q values. This indicates that thermoelastic damping alone cannot account for the observed dissipation. Further improvement in Q may require suppression of additional loss mechanisms, such as surface-related losses and defect-related losses. Therefore, the f_0Q product was used as a figure of merit for fair comparison. The measured f_0, Q, and f_0Q values for all measured resonators are summarized in Table SI of the supplementary material. Table I summarizes the f_0, Q, and f_0Q values of previously demonstrated β-Ga_2O_3-based MEMS resonators, including the doubly clamped beams demonstrated in this work. Our beams exhibited f_0Q values exceeding the highest reported values for transferred-flake-based doubly clamped beams and comparable to the highest reported values for transferred-flake-based circular drumhead resonators, highlighting the potential advantage of our crystallographic-etching-based fabrication technique.

We further analyzed the L dependence of f_0 to determine the Young's modulus (E) along the beam direction. The fundamental-mode f_0 of a doubly clamped beam without axial stress can be expressed using Euler–Bernoulli beam theory as[32]

$$f_0\left(L_{\mathrm{eff}}\right) = \frac{\beta_1^2 t}{2\pi L_{\mathrm{eff}}^2}\sqrt{\frac{E}{12\rho}},$$

where $L_{\mathrm{eff}} = L + \Delta L$ is the effective beam length, $\beta_1 = 4.730$ is the eigenvalue for the fundamental mode of a doubly clamped beam, and $\rho = 5.96\,\mathrm{g\,cm^{-3}}$ is the density of β-Ga_2O_3. Here, ΔL was used as a constant fitting parameter common to all beams, representing the correction to L. This correction accounts for possible deviations of the effective vibrating length from the measured L values, which may

© 2026 The Author(s). Published on behalf of
The Japan Society of Applied Physics by IOP Publishing Ltd

Table I. Specifications and figures of merit of demonstrated β-Ga_2O_3-based MEMS resonators. f_0 and Q denote resonant frequency and quality factor, respectively.

Resonator structure	Fabrication method	f_0 (MHz)	Q ($\times 10^2$)	f_0Q ($\times 10^{10}$ Hz)	References
Circular drumhead	Transfer of flakes grown by low-pressure chemical vapor deposition	10.0–74.9	0.98–8.26	0.147–4.24	Zheng et al.[19]
		30.2	15.3	0.462	Zheng et al.[21]
		29.6–47.7	2.44–6.26	0.806–2.52	Zheng et al.[20]
Doubly clamped beam	Transfer of exfoliated flakes from a bulk crystal	14.3	11.7	1.68	Zheng et al.[22]
		26.3	0.82	0.215	Zheng et al.[25]
		7.32–27.0	5.03–10.3	0.756–1.43	Zheng et al.[20]
		27.1	1.08	0.293	Zheng et al.[17]
		4.92–8.05	1.40–11.3	0.0688–0.908	Sui et al.[24]
Doubly clamped beam	Gas etching of a bulk crystal substrate	0.503–2.61	117–493	2.11–4.48	This work

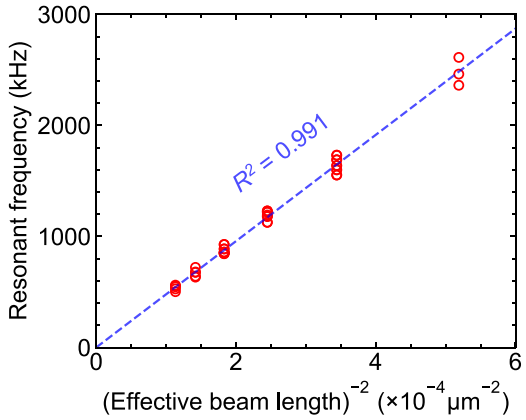


Fig. 3. Resonant frequency as a function of the inverse square of effective beam length. A fitted line is also shown.

arise from nonideal anchor geometry, slight elastic deformation of the clamping regions, and uncertainty in determining the beam edges from SEM images.

Based on this equation, the measured f_0–L relationship was fitted using

$$f_0(L) = \frac{C}{(L + \Delta L)^2},$$

where C and ΔL are fitting parameters. The fitting yielded $\Delta L = -3.60$ μm, from which L_{eff} was calculated. The resulting f_0–L_{eff}^{-2} plot exhibited excellent linearity, with $R^2 = 0.991$, as shown in Fig. 3. Because this linearity alone does not exclude a small residual axial stress, we additionally analyzed the f_0–L relationship using a model including both bending and axial stress. The analysis indicated only a small residual tensile stress, with a conservative upper estimate of approximately 17 MPa within the measured thickness range (see supplementary material). Therefore, the simpler bending-only model with ΔL was retained for the following effective-modulus analysis.

The effective Young's modulus was then extracted from the fitted coefficient C using

$$E = 12\rho\left(\frac{2\pi C}{\beta_1^2 t}\right)^2,$$

yielding a value of 143.2 (+16.4/−14.0) GPa within the Euler–Bernoulli beam approximation. The uncertainty originates from the measured beam thickness, t. Because the present beams have $w/t \approx 6$, a finite-width plane-strain effect may influence the extracted modulus. For an isotropic material, the corresponding correction factor is $1/(1-\nu^2)$, which corresponds to an increase of approximately 4%–10% for representative Poisson's ratios of 0.2–0.3. This magnitude is comparable to the difference between the extracted value and the reference Young's modulus of approximately 153 GPa along the [100] direction, derived from the reported elastic constants of β-Ga_2O_3.[33,34] Details of this calculation are provided in the supplementary material. However, because β-Ga_2O_3 is strongly elastically anisotropic, an accurate finite-width correction would require an anisotropic elastic analysis and cannot be obtained using a simple isotropic plate correction. Therefore, the extracted value should be regarded as an effective modulus within the present beam approximation.

For future monolithically integrated β-Ga_2O_3 MEMS resonators, an integrated transduction scheme will be required because centrosymmetric β-Ga_2O_3 does not exhibit intrinsic piezoelectricity. Possible approaches include electrostatic transduction using patterned electrodes and capacitive air gaps or piezoelectric transduction using a deposited piezoelectric thin film. β-Ga_2O_3 is an oxide with a high melting point of 2066 K,[35] suggesting good thermal robustness for high-temperature processing required for the deposition and crystallization of various piezoelectric thin films, including PZT films. In addition, the crystallographic gas etching used in this study was performed at 647 °C for only 11 min, providing flexibility in the process sequence. Thus, electrodes and piezoelectric layers could potentially be formed either before or after the gas-etching step, depending on their thermal and chemical stability. These features provide several possible routes toward integrated transduction, although the compatibility of specific transducer materials and device structures with the present etching process remains to be experimentally established.

In summary, this study demonstrated the resonance characteristics of monolithic β-Ga_2O_3-based MEMS resonators fabricated directly on a native substrate. The fabricated doubly clamped beams showed clear fundamental-mode resonance with Q values on the order of 10^4, confirming the mechanical functionality of the previously developed suspended structures. The beam-length-dependent resonance

© 2026 The Author(s). Published on behalf of The Japan Society of Applied Physics by IOP Publishing Ltd

analysis yielded an effective Young's modulus within the Euler–Bernoulli beam approximation. These findings provide an important basis for developing reproducible, monolithic β-Ga_2O_3 MEMS that can be integrated with other β-Ga_2O_3-based devices on the same material platform.

Acknowledgment This study was supported by the Nanofabrication Unit and Electron Microscopy Unit at the National Institute for Materials Science (NIMS) under the framework of the Advanced Research Infrastructure for Materials and Nanotechnology (ARIM), supported by the Ministry of Education, Culture, Sports, Science and Technology (MEXT), Japan (No. JPMXP1225NM5079, JPMXP1226NM5028). This work was financially supported by a Grant-in-Aid for Scientific Research from the Japan Society for the Promotion of Science (JSPS), Japan (No. JP24K00937, JP24K01368, JP24H00287).

ORCID iDs Takayoshi Oshima https://orcid.org/0000-0001-8550-9735; Yuichi Oshima https://orcid.org/0000-0001-8293-4891; Masataka Imura https://orcid.org/0000-0002-4236-9549; Meiyong Liao https://orcid.org/0000-0003-1361-4266; Ya Zhang https://orcid.org/0000-0001-6108-5261

1) H.-P. Phan, D. V. Dao, K. Nakamura, S. Dimitrijev, and N.-T. Nguyen, J. Microelectromech. Syst. **24**, 1663 (2015).
2) Q. Zhang, Y. Liu, H. Li, J. Wang, Y. Wang, F. Cheng, H. Han, and P. Zhang, Sensors **24**, 7731 (2024).
3) M. Rais-Zadeh, V. J. Gokhale, A. Ansari, M. Faucher, D. Theron, Y. Cordier, and L. Buchaillot, J. Microelectromech. Syst. **23**, 1252 (2014).
4) G. Chen, S. Koizumi, Y. Koide, and M. Liao, Accounts Mater. Res. **5**, 1087 (2024).
5) Y. Tao, J. M. Boss, B. A. Moores, and C. L. Degen, Nat. Commun. **5**, 3638 (2014).
6) T. Onuma, S. Saito, K. Sasaki, T. Masui, T. Yamaguchi, T. Honda, and M. Higashiwaki, Jpn. J. Appl. Phys. **54**, 112601 (2015).
7) T. Oshima, M. Hashikawa, S. Tomizawa, K. Miki, T. Oishi, K. Sasaki, and A. Kuramata, Appl. Phys. Express **11**, 112202 (2018).
8) B. Cromer et al., J. Vac. Sci. Technol. A **42**, 033206 (2024).
9) T. Oshima, T. Okuno, N. Arai, N. Suzuki, S. Ohira, and S. Fujita, Appl. Phys. Express **1**, 011202 (2008).
10) S. J. Pearton, F. Ren, A. Y. Polyakov, A. Haque, M. Labed, and Y. S. Rim, Appl. Phys. Rev. **12**, 031336 (2025).
11) M. Bartic, Y. Toyoda, C.-I. Baban, and M. Ogita, Jpn. J. Appl. Phys. **45**, 5186 (2006).
12) S. Jang, S. Jung, J. Kim, F. Ren, S. J. Pearton, and K. H. Baik, ECS J. Solid State Sci. Technol. **7**, Q3180 (2018).
13) C. Hou, K. R. York, R. A. Makin, S. M. Durbin, R. M. Gazoni, R. J. Reeves, and M. W. Allen, Appl. Phys. Lett. **117**, 203502 (2020).
14) A. E. Islam et al., Appl. Phys. Lett. **121**, 243501 (2022).
15) M. H. Wong, A. Takeyama, T. Makino, T. Ohshima, K. Sasaki, A. Kuramata, S. Yamakoshi, and M. Higashiwaki, Appl. Phys. Lett. **112**, 023503 (2018).
16) S. A. Khan, S. Saha, U. Singisetti, and A. F. M. A. U. Bhuiyan, J. Appl. Phys. **136**, 225701 (2024).
17) X.-Q. Zheng, H. Zhao, and P. X. L. Feng, Appl. Phys. Lett. **120**, 040502 (2022).
18) L. Huang, H. Tang, C. Zhang, P. Sun, Q. Fang, F. Wu, P. Luo, B. Liu, and J. Xu, Eur. Phys. J. Spec. Top. **234**, 231 (2025).
19) X.-Q. Zheng, J. Lee, S. Rafique, L. Han, C. A. Zorman, H. Zhao, and P. X. L. Feng, ACS Appl. Mater. Interfaces **9**, 43090 (2017).
20) X.-Q. Zheng, H. Zhao, Z. Jia, X. Tao, and P. X. L. Feng, Appl. Phys. Lett. **119**, 013505 (2021).
21) X.-Q. Zheng, J. Lee, S. Rafique, M. R. Karim, L. Han, H. Zhao, C. A. Zorman, and P. X. L. Feng, IEEE Electron Device Lett. **39**, 1230 (2018).
22) X.-Q. Zheng, Y. Xie, J. Lee, Z. Jia, X. Tao, and P. X. L. Feng, APL Mater. **7**, 022523 (2019).
23) M.-F. Yu, M. Z. Atashbar, and X. Chen, IEEE Sens. J. **5**, 20 (2005).
24) W. Sui, S. M. E. H. Yousuf, Y. Liu, S. J. Pearton, and P. X. L. Feng, Adv. Mater. Technol. **9**, 2301356 (2024).
25) X.-Q. Zheng, T. Kaisar, and P. X.-L. Feng, Appl. Phys. Lett. **117**, 243504 (2020).
26) M. Peres et al., ECS J. Solid State Sci. Technol. **8**, Q3235 (2019).
27) T. Oshima and Y. Oshima, AIP Adv. **15**, 055207 (2025).
28) T. Oshima and Y. Oshima, Sci. Tech. Adv. Mater. Meth. **5**, 2554046 (2025).
29) T. Oshima, Appl. Phys. Express **18**, 116501 (2025).
30) K. Adachi, N. Watanabe, H. Okamoto, H. Yamaguchi, T. Kimoto, and J. Suda, Sensors Actuators A **197**, 122 (2013).
31) Y. Chen, L. Sang, S. Koizumi, Y. Koide, X. Liu, and M. Liao, Diam. Relat. Mater. **129**, 109340 (2022).
32) K. L. Ekinci and M. L. Roukes, Rev. Sci. Instrum. **76**, 061101 (2005).
33) K. Adachi, H. Ogi, N. Takeuchi, N. Nakamura, H. Watanabe, T. Ito, and Y. Ozaki, J. Appl. Phys. **124**, 085102 (2018).
34) S. Poncé and F. Giustino, Phys. Rev. Res. **2**, 033102 (2020).
35) K. Hoshikawa, E. Ohba, T. Kobayashi, J. Yanagisawa, C. Miyagawa, and Y. Nakamura, J. Cryst. Growth **447**, 36 (2016).

© 2026 The Author(s). Published on behalf of The Japan Society of Applied Physics by IOP Publishing Ltd